Galerkin-Method Approach to Nonlinear Soliton Classical Stability

C. A. Linhares and H. P. de Oliveira
Departamento de Física Teórica - Instituto de Física A. D. Tavares
Universidade do Estado do Rio de Janeiro
CEP 20550-013 Rio de Janeiro – RJ, Brazil

Received on 4 December, 2006

We examine the evolution of perturbations on the kink configuration in $\lambda\phi^4$ theory and of the Nielsen–Olesen vortex in scalar electrodynamics through the Galerkin method. The problem is reduced to a finite dynamical system for which the linear and nonlinear regimes are studied. The linear stability of both is associated to a motion in a stable torus present in phase space, whereas the nonlinear evolution of perturbations can be viewed as a consequence of the breakdown of the tori structure and the onset of chaos. We discuss this regime in connection with the stability of the configurations. Also, the Galerkin method is used to obtain approximate analytical expressions for the vortex profile.

Keywords: Stability of solitons; Nielsen-Olesen vortex; Galerkin model

I. INTRODUCTION

One of the main features of soliton (solitary wave) solutions of nonlinear differential equations is the permanence of its shape in time. Besides this formal and important aspect, solitonic configurations are present in many areas of physics, besides the original one in hydrodynamics [1]. For instance, we may cite in elementary particle physics where solitons may be regarded as extended particlelike solutions of nonlinear field equations of various types, providing well-known configurations such as the kink solution in ϕ^4 or sine–Gordon theory, or as vortices and monopoles in gauge field theories [2]. In cosmology, extended configurations like cosmic strings and domain walls are considered as possible candidates of dark matter [3]. Importantly, also, in condensed-matter physics, solitons may appear as fluxons present in the Josephson junction transmission line [4]. Many other examples are studied in the literature.

Much attention has been given to the study of the behavior of solitons under the influence of some perturbations, in which the very first approach was focused on linear perturbation theory [2],[5]-[9]. Physically, such perturbations represent the interaction between the soliton with very small spatial inhomogeneities which, in the case of condensed matter, may be thought of as impurities or defects typical even in the purest material samples. On the other hand, it can happen that the spatial inhomogeneities are not restricted to be small, and therefore the problem of their interaction with solitary waves naturally emerges. In this situation, the basic difficulty is the inner complexity of the problem due to the high degree of nonlinearity present even in the most simple differential equations of interest. Therefore, most analysis on soliton stability relied entirely on numerical methods or were restricted to the linear order of perturbation theory.

Nonlinearities are also the main reason for the impossibility of determining analytical expressions for the functions which define solitonic configurations of field theories in more than one spatial dimensions, such as vortices in gauge theories, even in the static case. These are again obtained usually through numerical calculations, and these seem to be inevitable for the discussion of stability of these configurations under small perturbations.

Our purpose in the present article is to approach the subject so that the contributions from nonlinear terms in the differential equations are more explicitly controlled. To this end, we apply the so-called 'traditional Galerkin method' [10, 11], of wide applications to nonlinear problems encountered, for instance, in the physics and engineering of dynamical fluids (for a recent reference see [12]). Although it provides only approximate solutions to the differential equation one wishes to study, and in the end one needs to resort to numerical calculations, the method is able to produce some more analytical information on the problem, and in a few situations it may be completely solved by a symbol-manipulating computer language.

The Galerkin method starts by postulating a solution in spacetime to a partial differential equation in the form of a finite series of an arbitrary set of space-dependent functions, which are chosen to suit the boundary conditions of the problem, multiplied by time-dependent coefficients. By inserting this trial solution into the differential equation and projecting onto the same set of functions, one gets a system of ordinary differential equations in time for the series coefficients. This last system is then solved numerically, providing the time evolution of the coefficients. In the simpler static case, the coefficients are just numbers, and the last system to solve is an algebraic one. In both situations, the number N of terms in the series is however also arbitrary, and it must be decided upon according to the desired numerical accuracy. This defines a truncation of a possibly infinite series, which is then differently approximated for different choices of N. One expects that for growing N the approximation converges to the true solution, and this feature is illustrated below for the specific problems we study.

The evolution in time of perturbations of solitonic configurations are known to have chaotic properties under adequate conditions [13, 14]. In those studies, a Painlevé analysis is carried out on the simplified case of spatially homogeneous fields. With our Galerkin approach, however, we were able of handling the more general case of varying fields in both time

and space.

In this paper we apply the approach outlined above to topological configurations appearing in two relativistic classical field theories. It is organized as follows. In Section 2, we consider the topological kink found in (1+1)-dimensional scalar field theory with quartic potential in the broken-symmetric phase. We study its stability by adding to it a general perturbation function in spacetime with an initial Gaussian shape. The perturbation is then made to evolve according to the field equation of the theory (sometimes called the 'nonlinear Klein–Gordon equation'), of which we keep all nonlinear terms, and treat it following the Galerkin prescription. The analysis of the results we have obtained from the numerical integration of the system of ordinary differential equations for Galerkin coefficients then ensues. We also exhibit there the power spectrum of the perturbed field, for which an average over the space coordinates is taken, showing the typical features of a transition to a chaotic behavior. In Section 3, we turn first to the Nielsen–Olesen static vortex configuration of scalar electrodynamics, which may play a role in the description of superconducting phase transitions [15] or even in cosmic strings scenarios [16]. As far as we know, there is still lacking in the literature a closed analytical expression for it. Thus, before tackling the study of vortex perturbations, we had here to establish the two radial functions on a plane satisfying a system of coupled nonlinear partial differential equations of which the vortex is a solution. We are able to solve completely the Galerkin algebraic system, providing expressions, for each value of the topological charge, of the functions which define the vortex shape. The question of the vortex stability under time-dependent perturbations of these functions is studied next. Finally, in the last Section we conclude. In the Appendix we present a few Galerkin-constructed static Nielsen–Olesen vortices for varying characteristic parameters and topological numbers.

II. NONLINEAR PERTURBATIONS OF THE KINK SOLUTION

A. Basic Galerkin approach to the kink and its perturbations

We here consider the evolution of perturbations of the usual kink solution of a real scalar field theory with potential $V(\phi) = \frac{1}{4}\left(\phi^2 - b^2\right)^2$ in (1+1)-dimensional spacetime, where b is a constant which parametrizes the spontaneous symmetry breakdown. The field equation for that theory in reads

$$\left(\frac{\partial^2}{\partial t^2} - \frac{\partial^2}{\partial x^2}\right)\phi(x,t) + \left(\phi(x,t)^2 - b^2\right)\phi(x,t) = 0. \qquad (1)$$

Its (static) kink solution has the form

$$\phi_0(x) = b\tanh\frac{b}{\sqrt{2}}x, \qquad (2)$$

where the space coordinate x runs from $-\infty$ to $+\infty$. We study the behavior of general perturbations of this kink solution by writing

$$\phi(x,t) = \phi_0(x) + \delta\phi(x,t). \qquad (3)$$

For the sake of convenience, we introduce a new spatial variable $\xi \equiv \tanh\left(bx/\sqrt{2}\right)$, so that the interval $-\infty < x < +\infty$ corresponds to $-1 < \xi < 1$ and the unperturbed kink is now described as $\phi_0(\xi) = b\xi$. After rewriting the field equation (1) for the ξ variable, we introduce Eq. (3) onto it, and obtain a differential equation for the perturbation $\delta\phi(x,t)$:

$$(\delta\phi)^{\cdot\cdot} - \frac{b^2}{2}(1-\xi^2)\left[\left(1-\xi^2\right)(\delta\phi)'' - 2\xi(\delta\phi)'\right] + \left(3\xi^2 - 1\right)b^2\,\delta\phi + (3b\xi + \delta\phi)(\delta\phi)^2 = 0, \qquad (4)$$

where the prime means derivative with respect to ξ. If one wishes to restrict the problem to linear perturbations, it is then necessary to drop the last term in the lhs of Eq. (4). A complete analysis of this case can be found in Ref. [7].

We seek instead solutions to the complete equation (4), for which we implement the Galerkin procedure [10]. Also, we adopt the following boundary conditions[7] to be satisfied by the perturbation $\delta\phi$:

$$\delta\phi(\xi = \pm 1, t) = 0, \qquad (5)$$

which is equivalent to $\delta\phi(x = \pm\infty, t) = 0$. The Galerkin method postulates an approximate solution (the 'trial' solution) for the equation as a finite sum, which in our case the perturbation $\delta\phi$ may be written

$$\delta\phi(\xi,t) = \sum_{k=0}^{N} a_k(t)\psi_k(\xi), \qquad (6)$$

where the ψ_k constitute a set of analytic basis functions, to be chosen suitably, as a generalization of a Fourier expansion, and N is the order of the series truncation. It remains therefore to compute the $N+1$ 'modal' coefficients $a_k(t)$.

Our choice of basis functions, which satisfy the boundary conditions, is

$$\psi_k(\xi) = T_{k+2}(\xi) - T_k(\xi), \qquad (7)$$

where $T_k(\xi)$ is the Chebyshev polynomial of degree k. Properties of Chebyshev polynomials are well-known (see, for instance, [17]); the main one for our purposes is that they are orthogonal in the interval $(-1,1)$ over a weight $(1-\xi^2)^{-1/2}$.

The behavior of the modal coefficients $a_k(t)$ are dictated by the equations resulting from the following steps: (i) introduce the decomposition (6) into the lhs of Eq. (4), so that it produces an expression known by the residual equation, $\mathrm{Res}(\xi,t) \simeq 0$, for which the equality is attained only for the exact solution ($N \to \infty$); (ii) project the residual equation onto each mode $\psi_j(\xi)$, for all $j = 0,\ldots,N$, through the operation $\langle \mathrm{Res}, \psi_j \rangle \equiv \int_{-1}^{1} d\xi\, \mathrm{Res}(\xi,t)\psi_j$. The Galerkin method establishes that each projection must vanish, i. e., $\langle R, \psi_j \rangle = 0$, $j = 0,1,..,N$. We then obtain a set of ordinary differential equations involving the modal coefficients and their second-order time derivatives. After solving this set of equations for

the second-order time derivatives (this is necessary since the basis functions $\psi_k(\xi)$ are not orthogonal), it follows that

$$\ddot{a}_0(t)+\frac{5}{2}a_0(t)^3+\frac{b^2}{2}a_2(t)+\frac{23595b^2}{7429}a_{10}(t) +\cdots=0$$

$$\ddot{a}_1(t)+\frac{3b^2}{2}a_1(t)+\frac{44987b^2}{63365}a_{11}(t)+\cdots=0$$

$$\ddot{a}_2(t)+\frac{11b^2}{4}a_2(t)-\frac{3b^2}{4}a_4(t)+\frac{16335b^2}{1748}a_{10}(t) +\cdots=0$$

$$\vdots$$

$$\ddot{a}_{11}(t)-\frac{63b^2}{4}a_9(t)+\frac{3701b^2}{58}a_{11}(t)+\cdots=0,$$

for the $N=11$ case. Since each of the above equations has typically more than 200 terms (a number which grows for increasing N), with all kinds of square and cubic combinations of the modal coefficients, we have just displayed the linear terms, except for the cubic term in the first equation. As a matter of fact, it is possible to envisage the behavior of the linear perturbations in a very simple way, as well as to give an account of the effect of the nonlinearities for a more general perturbation using our dynamical system approach. For instance, in the case of linearized perturbations the set of equations for $a_1(t),a_2(t),..,a_N(t)$ are reduced to coupled harmonic oscillators for which there is no contribution from $a_0(t)$. Then, once the $a_k(t)$, $k=1,2,...,N$, are known, the evolution of $a_0(t)$ is then determined. It should be noticed that in all equations, including the one for $\ddot{a}_0(t)$, the linear term in a_0 is lacking. This peculiar aspect of the linearized equations is a consequence of the existence of a static configuration characterized by $a_0=$ const., $a_1=a_2=...=a_N=0$, as we are going to see.

In order to perform the numerical experiments we need to fix the initial values for the modal coefficients $a_k(0)$, $k=0,\ldots,N$, which determine the initial strength of the perturbation $\delta\phi_0(\xi)=\delta\phi(\xi,0)$. We may, for instance, take a Gaussian initial profile such that

$$\delta\phi_0(\xi)=\frac{A_0}{\sqrt{2\pi}\sigma}\exp\left[-\frac{1}{2\sigma^2}\left(x(\xi)-x(\xi_0)\right)^2\right], \qquad (8)$$

where σ is the standard deviation, $x(\xi_0)$ and A_0 are the center and the strength of the distribution, respectively. Note that this initial profile satisfies the established boundary conditions. The initial values of the modal coefficients are determined from the Galerkin decomposition of Eq. (8), or

$$\delta\phi_0(\xi)=\sum_{k=0}^{N}a_k(0)\,\psi_k(\xi). \qquad (9)$$

Each value of $a_k(0)$ is determined by projecting the above expression into the basis functions $\psi_k(\xi)$. By adjusting the control parameter A_0 (once x_0 and σ are fixed), it is possible to study the evolution of infinitesimal and more general perturbations as well. Fig. 1(a) illustrates schematically the kink solution plus the initial profile of the perturbation, whereas in Fig. 1(b) we plot $\delta\phi_0$ and $\sum_{k=0}^{N}a_k(0)\,\psi_k(\xi)$ for a few distinct values of N.

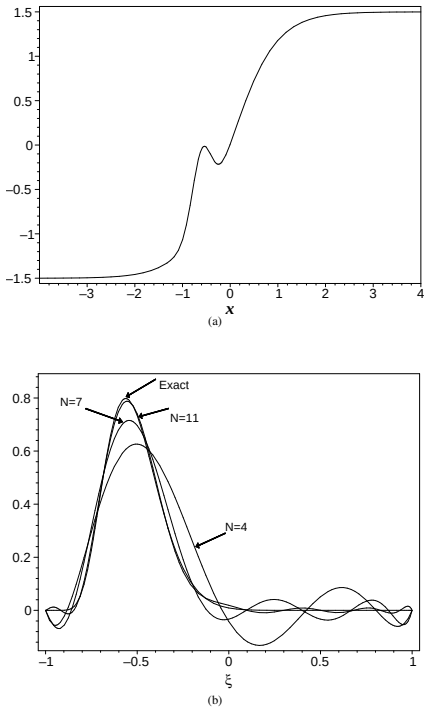

FIG. 1: (a) Plot of the kink plus the initial Gaussian perturbation (8). Here we have set $A_0=0.4$ and $b=1.5$ in order to illustrate the effect of the perturbation. (b) Plots of $\delta\phi_0(\xi)$ together with their Galerkin decompositions $\sum_{k=0}^{N}a_k(0)\psi_k(\xi)$ for $N=$4,7 and 11. We remark the effect of increasing N in almost describing the exact initial profile.

B. Numerical results

We present now the numerical evolution of perturbations determined by the Gaussian profile (8), where we have set $b=1.5$, $\xi_0=-0.562$, $\sigma=0.2$, and also assuming the truncation $N=11$. In the first numerical experiment we have chosen $A_0=0.01$, implying that $|a_k(0)|\sim 10^{-3}$–10^{-4}, therefore characterizing infinitesimal perturbations whose dynamics is basically dictated by the linear terms of Eq. (4). The results can be summarized as follows: (i) all $N+1$ modal coefficients have oscillatory behavior whatsoever the order of truncation N and the corresponding amplitudes are of the order of their own initial value; (ii) all other modal coefficients oscillate about zero; the exception is the first modal coefficient $a_0(t)$ which oscillates about a fixed value. Therefore, as expected, we infer that the kink is actually stable under small perturbations, as already pointed out by previous analytical studies on the linear perturbation theory [7].

The second aspect is in connection with the existence of the static solution

$$\delta\phi_{\rm static}=a_{\rm st}\psi_0(\xi)=a_{\rm st}(\xi^2-1), \qquad (10)$$

with $a_{\rm st}$ being a constant. Expressing the above solution back in the variable x, it follows that $\delta\phi_{\rm static}=-a_{\rm st}{\rm sech}^2\left(bx/\sqrt{2}\right)$, which is the only static solution of the linearized version of

Eq. (4). Actually, this solution accounts for the bound state in the zero or translational mode of the soliton, in accordance with Goldstone's theorem [6]. The sum $\psi(\xi) + p\ \delta\phi_0(\xi)$ corresponds to a soliton (or an antisoliton) which is translated by an amount proportional to p. In this way, the perturbation $\delta\psi(\xi,t)$ oscillates about the static configuration, meaning that the soliton $\psi(\xi) + p\ \delta\phi_0(\xi)$ is stable under small perturbations. In Fig. 2 we show the behavior of $a_0(t)$ and one of the other modes, say, $a_3(t)$.

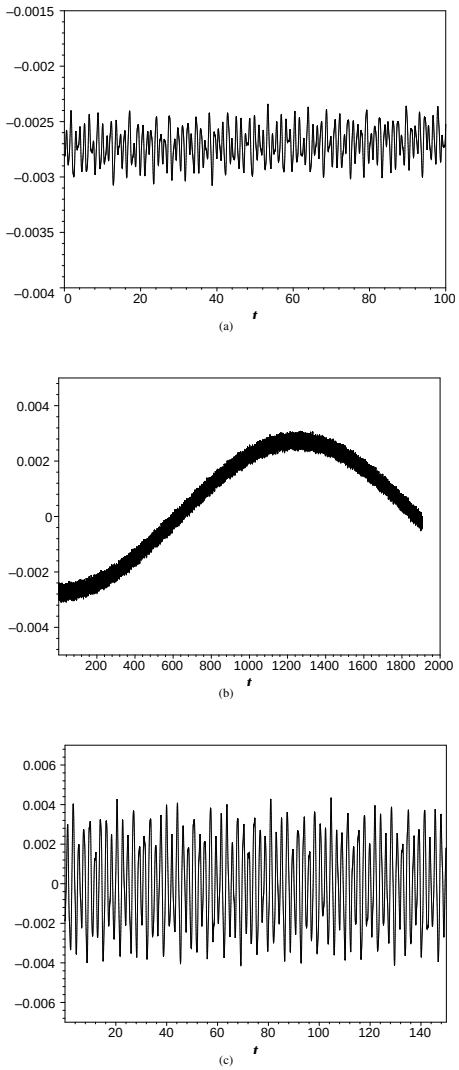

FIG. 2: Evolution of $a_0(t)$ with the choice $A_0 = 0.01$ in the intervals (a) $0 \le t \le 100$ and (b) $0 \le t < 2000$. Besides the rapid oscillations about the starting value $a_0 \simeq -0.0027$, there is another oscillating component with very small frequency about $a_0 = 0$. This feature can be understood as a consequence of the nonlinearities. The stability of the kink is however maintained. (c) oscillatory motion of $a_3(t)$, which is typical of any modal coefficient other than $a_0(t)$. These figures were obtained from the system of equations corresponding to the $N = 11$ truncation of the Galerkin expansion.

On the other hand, even in the case of small perturbations as described above, we have observed an interesting feature. The long time behavior of $a_0(t)$ reveals two types of oscillatory motion: one about $+a_{\rm st}$ or $-a_{\rm st}$, and another oscillatory motion between the soliton/antisoliton, $\pm a_{\rm st}$, with a very small frequency. Since this second type of oscillatory motion is absent in the linearized theory of perturbations, it may credited to the action of the nonlinearities. Though very small at the beginning, their influence takes place after a long time. In particular, this low-frequency component is due to the presence of the cubic term $\frac{5}{2}a_0(t)^3$, while the rapid oscillatory motion arises mainly from the contribution of all modal coefficients $a_k(t)$, $k \neq 0$.

The next step is to increase the value of the parameter A_0, breaking the linear approximation. As a matter of fact the nonlinearities enter into scene altering drastically the evolution of the modal coefficients producing a transition from regular to chaotic dynamics (cf. Fig. 3). A possible way to show such a transition consists in studying the power spectrum of the averaged scalar field evaluated directly from Eq. (3) $\langle\phi(x,t)\rangle$, instead of following the evolution of each modal coefficient. Then,

$$\langle\phi(x,t)\rangle = \int_{-\infty}^{\infty} \delta\phi(x,t)dx = -4\sum_{k=0}^{N} \frac{a_{2k}}{2k+1}, \qquad (11)$$

where we have taken into account the decomposition (3) and performed the change of variables from x to ξ. We have considered $A_0 = 0.008, 0.2, 0.7$, and the corresponding power spectra are show in Fig. 3. It is important to remark that the modal coefficients remain bounded, indicating the nonlinear stability of the kink.

In the first case, $A_0 = 0.008$ and the initial values of the modal coefficients are very small ($\sim 10^{-4} - 10^{-5}$). Accordingly, the resulting dynamical system is mainly dominated by the linear terms of Eq. (4), whose imprint in the power spectrum of $\langle\phi(x,t)\rangle$ is the existence of sharp peaks corresponding to well defined frequencies. At this point it will be very useful to interpret the dynamical system for the modal coefficients as a Hamiltonian system of $N+1$ degrees of freedom. In this vein, the corresponding phase space of all possible solutions which satisfy the boundary conditions has $2(N+1)$ dimensions ($N+1$ modal coefficients plus $N+1$ conjugated momenta). In the case of very small perturbations, the overall dynamics of the modal coefficients is associated to the motion of an orbit in this phase space that belongs to an $(N+1)$-dimensional torus. The power spectrum shown in Fig. 3(c) is characterized by peaks that indicate the leading frequencies of the torus. Therefore, the stability of the kink under small perturbations can be associated to the motion of an orbit confined to an $(N+1)$-dimensional torus in the phase space under consideration.

By setting $A_0 = 0.2$, the initial values of the modal coefficients are considerably greater than in the previous case. The action of the nonlinearities becomes more effective and the dynamics of the modal coefficients starts to display a stochastic pattern, which is reflected in the power spectrum of $\langle\phi(x,t)\rangle$. We observe a strong component at zero frequency,

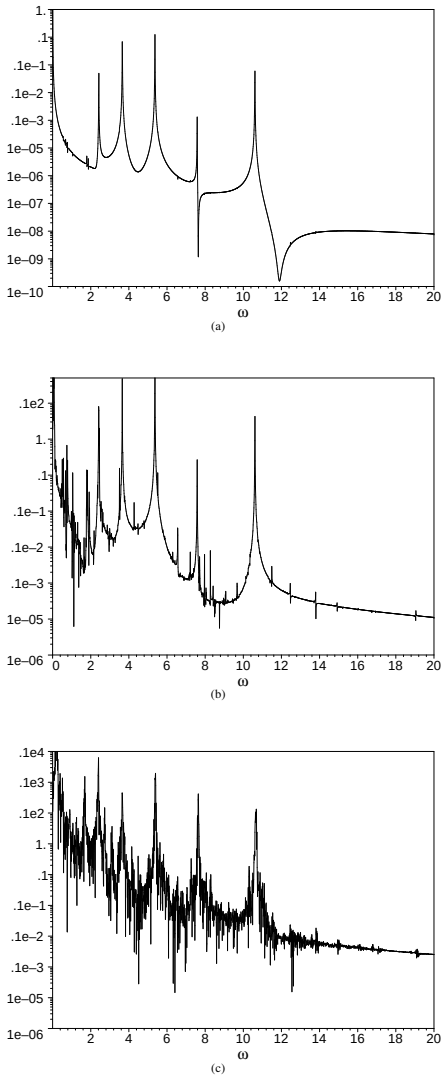

FIG. 3: Power spectra of $\langle\phi(x,t)\rangle$ for $A_0 = 0.008, 0.2, 0.7$ shown, respectively, in (a), (b) and (c). It is clear the transition from regular (quasiperiodic) to chaotic behavior with the break up of peaks and the emerging noise-like spectrum.

together with the appearance of a considerable range of frequencies, which starts to produce a noisy character in the power spectrum. In other words, this means that the structure of tori starts to break up producing eventually a chaotic dynamics. Since the leading frequencies are the same of the quasi-integrable case, the evolution of the modal coefficients is still close to the torus shown in Fig. 3(a).

In a more general situation, $A_0 = 0.7$, we note that a larger band of frequencies located between the peaks emerges in the power spectrum of $\langle\phi(x,t)\rangle$. This power spectrum, as shown in Fig. 3(c), indicates the stochastic character of the evolution of the perturbations. From the Hamiltonian point of view, this dynamics is produced by an orbit exploring randomically the portion of the phase space in a nonlinear neighborhood of the

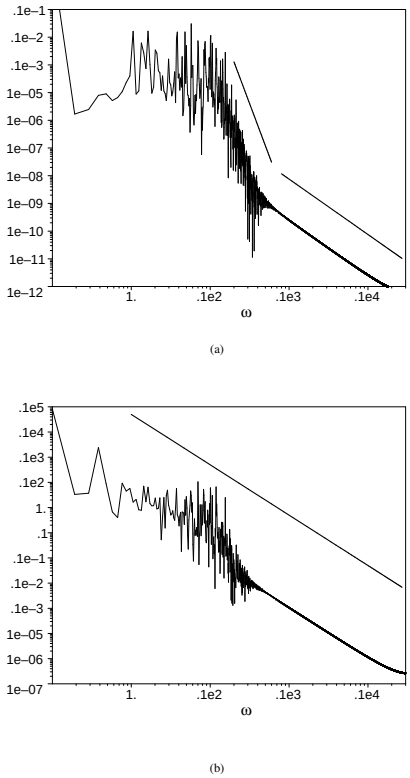

FIG. 4: Power spectra of $R(t)$ for $A_0 = 0.008, 0.7$ shown, respectively, in (a) and (b).

origin (kink), and therefore is a consequence of the bounded oscillatory behavior of all modal coefficients. This fact can be understood as an evidence of the stability of the kink under nonlinear perturbations.

The above results have shown that the increase of the initial perturbation induces the modal coefficients to exhibit a transition from quasi-periodic to chaotic behavior. Nevertheless, another interesting feature of the overall dynamics of perturbations about the kink can be undertaken by the power spectrum of the 'radius' defined in the space spanned by the modal coefficients,

$$R(t) = \left(\sum_{k=0}^{N} a_k^2 \right)^{\frac{1}{2}},$$

where the origin $R = 0$ represents the kink. In Fig. 4 we depict the power spectrum of $R(t)$ for the linear and nonlinear perturbations[1] characterized by $A_0 = 0.008$ and $A_0 = 0.7$, respectively. The first aspect worth mentioning is that in both cases the high-frequency spectrum satisfies a power law ω^{-k}, with $k \approx 2$, albeit the modal coefficients evolve in quite distinct

[1] By 'linear' perturbations we mean those small enough to reproduce the results of linear perturbation theory, although we keep all nonlinear terms in the computations.

regimes. This constitutes a self-similarity with respect to the strength of the perturbation. On the other hand, the effect of increasing the parameter A_0 is to change the power-law scaling present in the low-frequency domain (cf. Fig. 4(a)), for which the exponent changes from $k \approx 7.1$ to $k \approx 2$. In this situation the entire power spectrum seems to satisfy a power-law scaling as suggested by Fig. 4(b).

III. PROFILE AND STABILITY OF NIELSEN–OLESEN VORTICES

A. The static solution

In this subsection we employ the Galerkin method in order to establish the functional profile of a two-dimensional soliton: the Nielsen–Olesen vortex [20], which arises as a possible static classical configuration for the gauge field in scalar electrodynamics (also known as the Abelian Higgs model) in the broken-symmetric phase of the scalar field. A complete analytical solution for the description of the vortex field is not available in the literature, and its profile is known through numerically solving the field equations of the model (in the static limit and in a particular gauge). However, the asymptotic behavior at long distances and at the origin are known from requirements from finite energy and flux quantization, thus providing suitable boundary conditions for the construction of a solution.

In the present case we have to deal with a coupled system of nonlinear differential equations, for which an application of the Galerkin method may contribute to obtaining a solution in a different perspective from that of pure numerical integration. The method postulates an analytical form for the approximate solution of differential equations as a finite series on an adequate basis of functions. It remains therefore to compute the series coefficients, which is done numerically. In the case of the static Nielsen–Olesen vortex, these are obtained from solving an algebraic system of equations.

We thus consider the Abelian Higgs model, given by the following Lagrangian density for interacting scalar and vector fields:

$$\mathcal{L} = -\frac{1}{4}F^{\mu\nu}F_{\mu\nu} + \left|D_\mu\phi\right|^2 - V\left(|\phi|\right), \tag{13}$$

where $F_{\mu\nu}(x) = \partial_\mu A_\nu(x) - \partial_\nu A_\mu(x)$, $D_\mu\phi(x) = \left(\partial_\mu + ieA_\mu(x)\right)\phi(x)$ and $V\left(|\phi|\right) = \lambda\left(|\phi|^2 - \phi_0^2\right)^2$; $\phi_0 \neq 0$ is the broken-symmetry parameter and e is the electric charge of the ϕ field. The equations of motion are

$$\partial_\mu F^{\mu\nu} + 2e^2\left|\phi\right|^2 A^\nu = -ie\left(\phi^*\partial^\nu\phi - \phi\partial^\nu\phi^*\right), \tag{14}$$

$$D_\mu D^\mu\phi(x) = -2\lambda\phi\left(|\phi|^2 - \phi_0^2\right). \tag{15}$$

We are interested in the evolution vortex solution with cylindrical symmetry of the type

$$\mathbf{A}(r,\theta,t) = \hat{\theta}A(r,t) = \hat{\theta}\frac{n}{er}\left[1 - F(r,t)\right], \tag{16}$$

$$\phi(r,\theta,t) = \rho(r,t)e^{in\theta}, \text{ for integer } n. \tag{17}$$

We here follow the notation of Huang's book [21]. The cylindrical coordinates (r,θ) are adopted in the xy plane, and one seeks a solution with cylindrical symmetry corresponding to a flux of vortex lines which is quantized in units of $2\pi/e$. We also introduce suitable dimensionless coordinates, $t \to e\phi_0 t$, $r \to e\phi_0 r$ and $\rho \to \rho/\phi_0$, such that the field equations become

$$-\frac{\partial^2 F}{\partial t^2} + \frac{\partial^2 F}{\partial r^2} - \frac{1}{r}\frac{\partial F}{\partial r} - 2\rho^2 F = 0, \tag{18}$$

$$-\frac{\partial^2 \rho}{\partial t^2} + \frac{\partial^2 \rho}{\partial r^2} + \frac{1}{r}\frac{\partial \rho}{\partial r} - \frac{n^2F^2}{r^2}\rho - 2\beta\rho\left(\rho^2 - 1\right) = 0, \tag{19}$$

where $\beta = \lambda/e^2$. The boundary conditions are

$$F(0) = 1, \text{ for } n \neq 0; \qquad \lim_{r\to\infty} F(r) = 0; \tag{20}$$

$$\rho(0) = 0; \qquad \lim_{r\to\infty} \rho(r) = 1, \tag{21}$$

and the asymptotic behaviors at the origin and infinity are (see [20, 21])

$$F(r) \overset{r\to 0}{\to} 1 - O(r^2), \qquad F(r) \overset{r\to\infty}{\to} \text{const. } r^{1/2}e^{-\sqrt{2}e\phi_0 r}, \tag{22}$$

$$\rho(r) \overset{r\to 0}{\to} \text{const. } r^n. \tag{23}$$

As mentioned previously, our foremost task is to implement the Galerkin method to solve the system of differential equations (18)-(19) corresponding to the static case. The idea is to recover in an efficient manner the profile of the Nielsen–Olesen vortex found only numerically, in other words providing an approximate analytical expression for the fields $F(r)$ and $\rho(r)$. The dynamical evolution around the static configuration will be subject of the next subsection. Then, we must first choose the basis of functions on which we will define the series expansion. We adopt the criterion that the basis should reflect the boundary conditions and asymptotic behaviors above. Therefore, we introduce the rational Chebyshev functions $TL_k(x)$, defined in the semi-infinite interval $[0,\infty)$, which are written in terms of ordinary Chebyshev polynomials $T_k(x)$ as [22]

$$TL_k(x) = T_k\left(\frac{x-1}{x+1}\right), \tag{24}$$

for all $k \geq 0$. We may then define the functions

$$\psi_k(r) \equiv (-1)^{k+1}\frac{1}{2}\left(TL_{k+1}(r) - TL_k(r)\right), \tag{25}$$

with the limiting property $\lim_{r\to\infty}\psi_k(r) = 0$, which reproduces the long-distance behavior of $F(r)$. Nevertheless, we wish that the basis also reflect the asymptotic behavior of $F(r)$ at the origin and this requirement leads us to use the basis functions defined by

$$\chi_k(r) = \frac{2k^2+2k+1}{4k+4}\psi_{k+1}(r) - \frac{2(k+1)^2+2k+3}{4k+4}\psi_k(r), \tag{26}$$

so that $\chi_k(r) \sim 1 - O(r^2)$ near the origin. We now postulate a solution $F(r)$ as the finite series with real numerical coefficients

$$F(r) = \sum_{k=0}^{N} a_k\chi_k(r). \tag{27}$$

The constraint $F(0) = 1$ then makes one of the coefficients, say a_N, to be expressed in terms of the remaining a_k's. As for the decomposition of the $\rho(r)$ function in some appropriate $\Phi_k(r)$ basis functions, we have its $r \to \infty$ behavior implemented in the form

$$\rho(r) = 1 + \sum_{k=0}^{N} b_k \Phi_k(r). \tag{28}$$

As already mentioned, we want to choose the $\Phi_k(r)$ in order to satisfy the boundary conditions, in particular near the origin, so we must require that $\Phi_k(r) \sim r^n$, where n is the topological charge. Thus we may choose a different basis for each value of n: for $n = 1$, we may take

$$\Phi_k(r) = \psi_{k+1}(r) + \frac{3+2k}{1+2k}\psi_k(r), \tag{29}$$

while for $n = 2$, $\Phi_k(r) = \chi_k(r)$, and so on. In all cases, $\lim_{r\to\infty} \Phi_k(r) = 0$ and therefore $\rho(r) \to 1$ at long distances. Also, we take the coefficient b_N in (28) to be related to the other coefficients through the condition $\rho(0) = 0$.

If we insert both the above series decompositions of functions into the set of differential equations (18), (19), and integrating the residuals together with $\chi_k(r)$ and weight function $1/r^{1/2}(r+1)$ in the range $[0,\infty)$, the whole set of coefficients a_k, b_k may be determined, resulting in profiles for $F(r)$ and $\rho(r)$ in qualitative accordance with Nielsen–Olesen [20] or Huang [21].

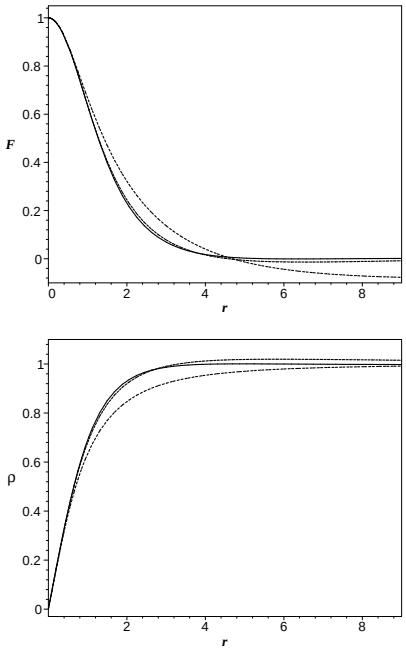

FIG. 5: Illustration of the rapid convergence of the Galerkin decompositions for F and ρ given by Eqs. (27) and (28), respectively. We have considered truncations $N = 3$ (dot), $N = 5$ (dash) and $N = 8$ (line).

We also wish to compare our results with the de Vega–Schaposnik exact $n = 1$ solution [23], obtained with the relation between coupling constants $e^2 = 2\lambda$ (in our notation). The result is that the de Vega–Schaposnik solution is accurately reproduced (see Figs. 1 and 2 of Ref. [23]) with just a few terms of the truncated series. In Figs. 5 (a) and (b) we see how this convergence is rapidly achieved for the solutions we have derived with the Galerkin method, with truncations $N = 3$, 5 and 8.

B. Nonlinear stability of the vortex

We proceed now with the investigation of the general dynamics of perturbations about the vortex configuration. For this task we use the Galerkin method to integrate the field equations (18) and (19), in which the decomposition of the fields $F(r,t)$ and $\rho(r,t)$ are the same as given by Eqs. (27) and (28) but assuming time dependence of the modal coefficients. The remaining steps to obtain the dynamical system are the same as already outlined previously. Thus, after a direct calculation we arrive at a set of equations of the form $\ddot{a}_k(t) = \mathcal{F}_k(a_j, b_j)$, $\ddot{b}_k(t) = \mathcal{G}_k(a_j, b_j)$, where $\mathcal{F}_k$ and $\mathcal{G}_k$ are nonlinear functions of the modal coefficients. Basically, as we have obtained in the case of the kink, these equations constitute a set of nonlinear coupled oscillators.

In the abstract phase space spanned by the modal coefficients (a_k, b_k), the static Nielsen–Olesen vortex is represented by a fixed point P_0 whose coordinates $(a_k^{(0)}, b_k^{(0)})$ were determined in the last subsection. To make arbitrary perturbations evolve about this configuration we set initial conditions of the type $a_k(0) = a_k^{(0)} + \delta a_k(0)$, $b_k(0) = b_k^{(0)} + \delta b_k(0)$, in order to include linear and nonlinear perturbations characterized by $|\delta a_k(0)/a_k^{(0)}|, |\delta b_k(0)/b_k^{(0)}| \ll 1$ and $|\delta a_k(0)/a_k^{(0)}|, |\delta b_k(0)/b_k^{(0)}| \sim O(1)$, respectively. The stability of the vortex will be guaranteed if the modes δa_k, δb_k remain bounded. Instead of studying the behavior of an averaged quantity associated to the perturbation we have considered the the 'radius'

$$R(t) = \left[\sum_{k=0}^{N-1} (\delta a_k^2 + \delta b_k^2)\right]^{\frac{1}{2}}.$$

In Fig. 6 we depict a log-linear plot of $R(t)$ corresponding to linear (graph at the bottom) and nonlinear (the next two graphs, for different initial strengths) perturbations about the Nielsen–Olesen vortex corresponding to $\beta = 0.5$, $n = 1$. Notice that $R(t)$ has a bounded oscillatory behavior which constitutes a good numerical evidence of the stability of the vortex beyond the linear perturbation scheme.

It is interesting that the three graphs look similar, apart from the amplitude of the oscillations and a low-frequency component present in the case of linear perturbations. We, then, proceed by examining the power spectrum of the radius as done in the case of perturbations about the kink. As we can see from Figs. 7, the whole power spectra exhibit a remarkable

self-similarity with respect to the initial strength of the perturbation. In particular note that domain of high frequencies satisfies a power-law scaling, ω^{-k}, with $k \approx 7.16$.

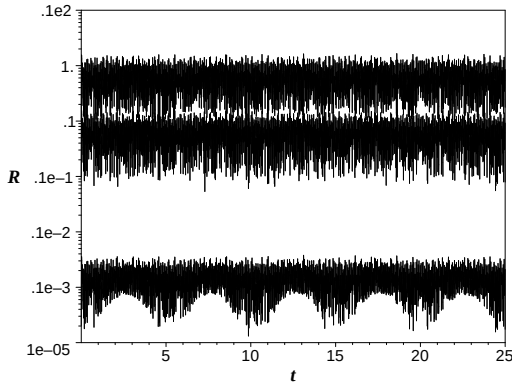

FIG. 6: Log-linear plot of the 'radius' versus time for linear and nonlinear perturbations (from the bottom to the top) about the vortex configuration. We have considered the case $\beta = 0.5$, $n = 1$ and truncation $N = 8$.

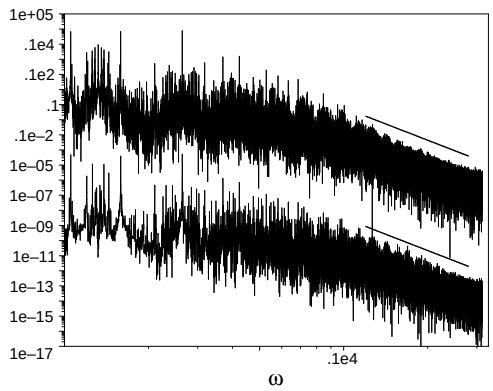

FIG. 7: Log-log plot of the power spectrum of $R(t)$ in the linear and nonlinear regime of the modal coefficients. The domain of high frequencies is well fitted with the power-law scaling ω^{-k} where $k \approx 7.16$. On the other hand, the effect of increasing the initial strength of perturbations reflects in the low-frequency range of the spectrum, where the peaks are split in a large number of components.

IV. CONCLUSIONS

In this paper we have studied the evolution of linear and nonlinear perturbations of the topological kink configuration of scalar field theories with quartic potential in the broken-symmetric phase, and of the Nielsen–Olesen vortex in scalar electrodynamics. We have applied the Galerkin method with two objectives in mind: (i) to reconstruct the Nielsen–Olesen vortex with a relatively low truncation order due to the appropriate choice of the trial functions $\chi_k(r)$ and $\Phi_k(r)$ (cf. Eqs. (26) and (29)); (ii) to tackle the nonlinear partial differential equations that govern the dynamics of arbitrary perturbations about the kink and the vortex static configurations. These equations were then approximated to dynamical systems in an abstract phase space according to the Galerkin method. In this phase space the solitonic configurations are represented by well-defined fixed points, and linear stability is guaranteed by the stable nature of these fixed points under small departures.

The numerical experiments have indicated that both solitonic configurations are indeed stable under nonlinear perturbations. In both cases very small perturbations may be interpreted as the motion of an orbit on a torus embedded in the phase space of the modal coefficients. The increase of the initial perturbation produces the transition from regular to chaotic by the breaking of the KAM torus (as suggested in Fig. 3), and possibly exhibiting Arnold diffusion which is typical in Hamiltonian systems with more than two degrees of freedom. The relevant consequence of this nontrivial dynamics emerges after constructing the power spectrum of the distance $R(t)$ from the fixed point representing the kink or the vortex. Then, from Figs. 4 and 7 we have shown that the power spectra satisfy a power law ω^{-k} valid within a large range of frequencies, where k assumes distinct values depending whether the kink or vortex perturbations are considered. The increase of the strength of initial perturbations seems not to alter the power law. There is thus the implication of self-similarity with respect to this increase. Therefore, the dynamics of perturbations about the solitonic configuration as described by $R(t)$ reveals to be complex, even though the modal coefficients evolve in the linear regime.

As our closing remarks, we believe that our approach has opened an fertile venue for treating the dynamics of nonlinear perturbations about the solitonic configurations under consideration. Physically, such nonlinear perturbations can be of interest in condensed-matter systems as well as in cosmology. As a next step, we intend to extend our analysis to the case of the 't Hooft–Polyakov monopole [24]. In this instance, it will be important to verify whether the self-similarity is also present in this other situation, along with trying to provide a clearer physical implication of such self-similarity. Finally, we must point out several works that were devoted to the study of chaos in gauge theories with vortices and monopoles solutions [25], in which the authors have used a different approximative scheme and have focused in the evaluation of the Lyapunov exponents associated to the soliton energy to characterize chaos.

APPENDIX A

In this appendix we present explicit expressions for the construction of static Nielsen–Olesen vortices through Galerkin expansions, as was explained in Section 3A. The two profile functions, $F(r)$ and $\rho(r)$, have expansions given by (27) and (28), respectively, for which we use different basis functions

χ_k and Φ_k, respectively (cf. Eqs. (25 and (28)). We have considered the truncation order $N = 8$, and after performing the Galerkin procedure a set of algebraic equations for the modal coefficients a_k and b_k is obtained. For the sake of completeness we exhibit the expressions of $F(r)$ and $\rho(r)$ corresponding to the case $\beta = 1/2$ parameter:

$$F(r) = 0.840376\,\frac{2r+1}{(r+1)^2} - 0.221538\,\frac{8r^2-3r-1}{(r+1)^3} - 0.0173983\,\frac{54r^3-145r^2+12r+3}{(r+1)^4} + 0.0214648\times \quad (A1)$$

$$\frac{32r^4-203r^3+161r^2-5r-1}{(r+1)^5} + 0.0026529\,\frac{5+30r-2010r^2+5376r^3-2835r^4+250r^5}{(r+1)^6} \quad (A2)$$

$$-0.000161889\,\frac{-21r+2530r^2-11682r^3+12969r^4-3817r^5+216r^6-3}{(r+1)^7} - 0.0004730614285714286\times \quad (A3)$$

$$\frac{7+56r-11011r^2+78078r^3-148863r^4+686r^7-17381r^6+92092r^5}{(r+1)^8} - \quad (A4)$$

$$0.00161165\,\frac{-1-9r+2695r^2-27209r^3+79365r^4+128r^8-4395r^7+33397r^6-84227r^5}{(r+1)^9} \quad (A5)$$

$$-\frac{0.00003385411}{(r+1)^{10}}\,(9+90r-38964r^2+531216r^3-2199834r^4+1458r^9-65127r^8+670752r^7 \quad (A6)$$

$$-2426580r^6+3568708r^5) \quad (A7)$$

$$\rho(r) = 1-1.1057\,(r+1)^{-2}+0.00809072\,\frac{5r-1}{(r+1)^3}+0.05115296\,\frac{35r^2-42r+3}{(r+1)^4}+0.01837782857142857\times \quad (A8)$$

$$,\frac{21r^3-63r^2+27r-1}{(r+1)^5} - 0.008523333\,\frac{5-220r+990r^2-924r^3+165r^4}{(r+1)^6} - 0.009276436363636364\times \quad (A9)$$

$$\frac{195r-1430r^2+2574r^3-1287r^4+143r^5-3}{(r+1)^7} - \frac{0.0009448492307692308}{(r+1)^8}\,(7-630r+6825r^2-20020r^3 \quad (A10)$$

$$+19305r^4+455r^6-6006r^5) + \frac{0.000175872}{(r+1)^9}\,(119r-1785r^2+7735r^3-12155r^4+85r^7-1547r^6+7293r^5 \quad (A11)$$

$$-1) + \frac{0.00003187141806342447}{(r+1)^{10}}\,(-1368r+27132r^2-162792r^3+377910r^4+969r^8-23256r^7+ \quad (A12)$$

$$151164r^6-369512r^5+9). \quad (A13)$$

By choosing other values of β the solution of the algebraic equations can be determined directly.

Acknowledgments H. P. O. acknowledges CNPq/Brazil for partial financial support. Figs. 2 were generated using the *Dynamics Solver* package [19].

[1] A. C. Scott, F. Y. F. Chu, and D. W. McLaughlin, Proc. IEEE **61**, 1443 (1973).

[2] R. Rajaraman, Phys. Rep. **21**, 227 (1975); *ibid., Solitons and Instantons*, North-Holland, Amsterdam, 1989.

[3] A. Vilenkin and E. P. S. Shellard, *Cosmic Strings and Other Topological Defects*, Cambridge University Press, Cambridge,

England, 1994.
[4] D. W. MacLaughlin and A. C. Scott, Phys. Rev. A **18**, 1652 (1978).
[5] T. I. Belova and A. E. Kudryavtsev, Physics-Uspekhi **40**, 359 (1997).
[6] M. B. Fogel, S. E. Trullinger, A. R. Bishop, and J. A. Krumhansl, Phys. Rev. B **15**, 1578 (1977).
[7] J. Rubinstein, J. Math. Phys. **11**, 258 (1970).
[8] N. R. Quintero and A. Sanchez, Eur. Phys. J. B**6**, 133 (1998).
[9] V. G. Makhankov, Phys. Rep. **35**, 1 (1978).
[10] C. A. J. Fletcher, *Computational Galerkin Methods*, Springer-Verlag, New York, 1984.
[11] D. Gottlieb and S. A. Orszag, *Numerical Analysis of Spectral Methods: Theory and Applications*, SIAM, Philadelphia, 1977.
[12] P. Holmes, J. L. Lumley, and G. Berkooz, *Turbulence, Coherent Structures, Dynamical Systems and Symmetry*, Cambridge University Press, Cambridge, UK, 1996.
[13] C. N. Kumar and A. Khare, J. Phys. A: Math. Gen. **22**, L849 (1989); B. Dey, C. N. Kumar and A. Sen, Int. J. Mod. Phys. A **8**, 1755 (1993).
[14] T. S. Biró, S. G. Matynian, and B. Müller, *Chaos and Gauge Field Theory*, World Scientific, Singapore, 1994.
[15] V. L. Ginzburg and L. D. Landau, Zh. Eksp. Teor. Fiz. **20**, 1064 (1950); L. P. Gorkov, Zh. Eksp. Teor. Fiz. **36**, 1364 (1959).
[16] M. Goodband and M. Hindmarsh, Phys. Rev. D **52**, 4621 (1995).
[17] W. H. Press, S. A. Teukolsky, W. T. Wetterling, and B. P. Flannery, *Numerical Recipes in C: The Art of Scientific Computing*, 2nd edition, Cambridge University Press, Cambridge, UK, 1992.
[18] A. R. Bishop, K. Fesser, and P. S. Lomdahl, Physica D **7**, 259 (1983).
[19] J. M. Aguirregabiria, *Dynamics Solver*, http://tp.lc.ehu.es/jma.html.
[20] H. B. Nielsen and P. Olesen, Nucl. Phys. B **61**, 45 (1973).
[21] K. Huang, *Quarks, Leptons & Gauge Fields*, World Scientific, Singapore, 1982.
[22] J. P. Boyd, *Chebyshev and Fourier Spectral Methods*, Dover, New York, 2001.
[23] H. J. de Vega and F. Schaposnik, Phys. Rev. D **14**, 1100 (1976).
[24] G. 't Hooft, Nucl. Phys. B **79**, 276 (1974); A. M. Polyakov, JETP Lett. **20**, 194 (1974),.
[25] T. Kawabe and S. Ohta, Phys. Rev. D **41**, 1983 (1990); Phys. Rev. D **44**, 1274 (1991); Phys. Rev. D **56**, 3660 (1997); Phys. Rev. D **61**, 105013 (2000).